THE JOURNAL OF PHYSICAL CHEMISTRY B LETTERS

2006, *110,* 36−41
Published on Web 12/10/2005

Shrinking Nanowires by Kinetically Controlled Electrooxidation

M. A. Thompson, E. J. Menke, C. C. Martens, and R. M. Penner*

Department of Chemistry and Institute for Surface and Interface Science, University of California, Irvine, California 92679-2025

Received: October 26, 2005; In Final Form: November 21, 2005

Nanowires composed of antimony, gold, and bismuth telluride (Bi_2Te_3) were reduced in diameter by electrooxidation in aqueous solutions. When electrooxidation was carried out using low current densities (J_{ox} < 150 μA cm^{-2}), the mean wire diameter decreased in direct proportion to the oxidation time, as expected for a kinetically controlled process. Under these conditions, the diameter uniformity of nanowires remained constant as wires were shrunk from initial diameters of more than 120 nm to less than 40 nm, for Sb and Bi_2Te_3, and less than 60 nm for Au. Oxidized nanowires remained continuous for more than 100 μm. Electrooxidation at higher current densities rapidly introduced breaks into these nanowires. Electrochemical wire growth and shrinking by electrooxidation were integrated into a single electrochemical experiment that allowed the final mean diameter of nanowires to be specified with a precision of 5−10 nm.

I. Introduction

Nanowires are of interest for a diverse range of applications including chemical sensors,[1−6] lasers,[7−10] thermoelectric generators,[11−15] and photodetectors.[16−20] Nanowire synthesis has generally involved "bottom-up" assembly from atomic or molecular precursors.[e.g.,21−25] The alternative, "top down", approach involves starting with a big wire and reducing its diameter into the nanometer range. One method for effecting this size reduction is using ion beam sputtering,[26] but it is unclear whether the dimensional uniformity present in the initial wire is retained during this size reduction process.

In this letter, we describe a new method for "shrinking" nanowires that permits the reduction of size to occur with precise control over the final nanowire diameter and with retention of the diameter uniformity present in the initial wire or distribution of wires. Our method involves the electrochemical oxidation of nanowires in solutions where the products of the oxidation are soluble. When the oxidation process is carried out slowly, under conditions of kinetic control, the time rate of change of the wire radius, dr/dt, becomes independent of the wire radius, thereby permitting nanowires to be reduced in diameter without roughening and without the introduction of breaks. In this letter, we present results for nanowires composed of three disparate materials: gold, antimony, and bismuth telluride (Bi_2Te_3) all synthesized using the electrochemical step edge decoration (ESED)[27] method.

II. Experimental Methods and Materials

The ESED syntheses of gold[28] and bismuth telluride,[12] but not antimony nanowires, have been previously described. Briefly, nanowire plating and electrooxidation experiments were carried out using a 50-mL glass and Teflon one-compartment, three-electrode cell using a platinum counter electrode and a saturated calomel reference electrode (SCE). Aqueous solutions were prepared using Nanopure water (ρ > 18 MΩ cm) and were purged with N_2 prior to each experiment. Nanowires were electrodeposited on the basal plane surface of ZYB-grade highly oriented pyrolytic graphite (HOPG, Advanced Ceramics, Inc., Cleveland, OH). A 10 × 10 × 1 mm^3 HOPG crystal was placed in a Teflon holder that exposed a circular area of approximately 0.20 cm^2 of the HOPG basal plane to the solution using an O-ring. The depositions were carried out using an EG & G 273A potentiostat/galvanostat.

The gold plating solution used was 2 mM $AuCl_3$ (Aldrich, 99.999%), 0.1 M KCl (Aldrich, 99.9+%), and 2 mM saccharin. The deposition was a typical three-pulse potentiostatic ESED program. Nanowires of antimony and gold were both prepared by applying three voltage pulses in succession (Scheme 1) as previously described.[28] For example, the three pulses required for the growth of gold nanowires were as follows: oxidation at HOPG step edges step at 0.80 V vs SCE for 5 s, nucleation at $E_{nucl} = -1.00$ V for $t_{nucl} = 125$ ms, and followed by growth at $E_{growth} = 0.45$ V_{SCE} for $t_{growth} = 30$ s. The corresponding parameters for the growth of antimony nanowires are summarized in Table 1. The electrodeposition solution for antimony was aqueous 5 mM $SbCl_3$ (Aldrich, 99.99+%), 0.1 M HNO_3, and 0.1 M tartaric acid (Aldrich, 98%). Bismuth telluride nanowires were prepared using a cyclic electrodeposition−stripping method identical to that described previously.[12] As indicated in Scheme 1, nanowire electrooxidation occurred immediately following electrodeposition and in the same solution. Electrooxidation potentials for each of the three materials explored here are listed in Table. 1.

Scanning electron microscopy (SEM) was carried out using a Philips FEG 30-XL microscope equipped with an EDAX elemental analyzer operating at an accelerating voltage of 20 keV.

III. Results and Discussion

During ESED nanowire electrodeposition, a constant, convection-controlled current, i_{growth}, is generally observed.[29] Under

* Address correspondence to: rmpenner@uci.edu.

10.1021/jp056160k CCC: $33.50

SCHEME 1: Pulse Program Used to Implement the Growth by ESED and Thinning of Metal Nanowires[a]

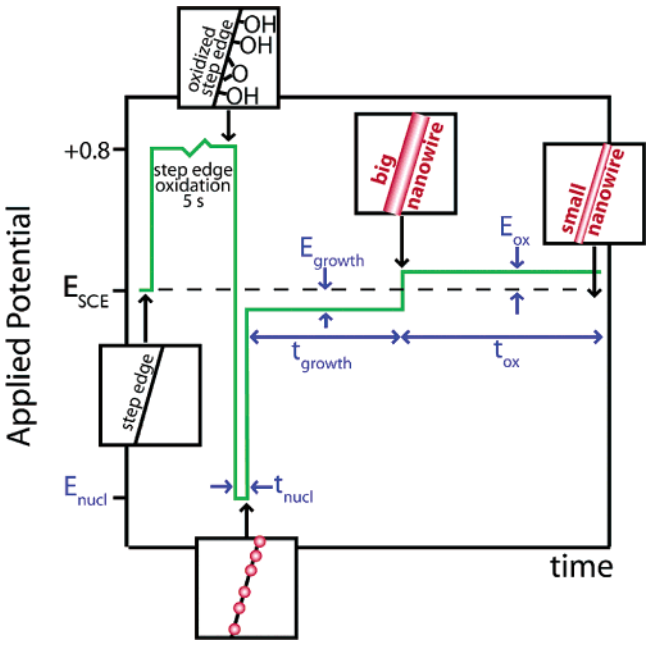

[a] The values of each parameter shown in blue are tabulated in Table 1.

these conditions, the increase in wire radius, $r(t)$, is approximately linear with the square root of the deposition time, $t_{growth}^{1/2}$. For a hemicylindrical wire of initial radius r_0, $r(t)$ is given by[25]

$$r(t) = r_0 + \sqrt{\frac{2i_{growth}t_{growth}V_m}{\pi nFl}} \quad (1)$$

where V_m is the molar volume of the deposited material, n is the number of electrons transferred per mole of deposited material, F is the Faraday constant (96485 C eq^{-1}), and l is the total length of nanowires present within 1 cm^2 of geometrical electrode area. The application of eq 1 to a distribution of nanowires with different radii (or a single nanowire of nonuniform radius) leads to narrowing of the diameter distribution as small nanowires (or constrictions in a particular nanowire) grow faster than large nanowires (or bulges in a particular nanowire).

For a kinetically controlled oxidation process of the type

$$M(s) \rightarrow M^{n+}(aq) + ne^- \quad (2)$$

a time-invariant oxidation current density, j_{ox}, is observed.[30,31] For a hemicylindrical wire, it is readily shown that $r(t)$ is given by

$$r(t) = r_{o2} - \frac{j_{ox}t_{ox}V_m}{nF} \quad (3)$$

where r_{o2} is the initial radius of a nanowire subjected to oxidation, and J_{ox} and t_{ox} are the oxidation current density and duration, respectively. If eq 3 is applied to the oxidation of an ensemble of nanowires with different radii (or to a single nanowire with a nonuniform radius), the radius of each nanowire (or the radius of each section along the axis of a particular nanowire) decreases in direct proportion to time with the result that standard deviation of the radius, σ_r, remains constant.

Coupling nanowire growth according to eq 1 with nanowire oxidation according to eq 3 provides a means for preparing dimensionally uniform nanowires of diminutive diameter. Consider the growth of a "rough" silver ($n = 1$, $V_m = 10.26$ cm^3 mol^{-1}) nanowire consisting of a linear ensemble of $r = 20$ nm hemispherical nanoparticles (Figure 1a, left). Within the context of the ESED experiment, this nanowire is produced by the nucleation of silver, followed by growth until these particles are, on average, tangential to one another (at the threshold of coalescence).[6,28] This nanowire has a mean radius, $\langle r \rangle = 15.7$ nm with $\sigma_r = 4.5$ nm and is characterized by the distribution of radii shown in Figure 1b (far left). Now, eq 1 can be used to predict the profile of this nanowire, as it is grown under conditions of constant total current. As shown in Figure 1a and b, growth under conditions of $i_{growth} = 10^{-9}$ A cm^{-2} for $t_{growth} = 600$ s produces a smoother nanowire with $\langle r \rangle = 65.8$ nm and $\sigma_r = 0.9$ nm; the wire radius has increased by a factor of 4, while its roughness has been reduced by 80% (Figure 1d). Equation 3 can then be used to propagate the wire radii distribution as this $\langle r \rangle = 65.8$ nm nanowire is oxidized ($n = 1$) under conditions of kinetic control using $J_{ox} = 10^{-4}$ A cm^{-2} for 500 s. The wire profile (Figure 1d) and the width of the radius distribution (Figure 1a,c) remain constant as $\langle r \rangle$ is reduced to 10.1 nm. In principle, t_{ox} can be extended with further shrinkage of $\langle r \rangle$ to approximately 3 nm before electrooxidation begins to introduce breaks.

This numerical calculation shows that a relatively large but "smoothed" nanowire resulting from ESED growth can be shrunk to 1/20th of its initial radius without inducing roughening and without introducing breaks. Can a similar result be achieved experimentally? We address this question now for nanowires composed of three disparate materials: gold (a noble metal), antimony (a base metal), and bismuth telluride (Bi_2Te_3, a compound). Nanowires of all three materials with diameters in the 120−150 nm range were prepared using the ESED method we have previously described.[12,28] The conditions of solution composition, applied potentials, and growth durations are summarized in Table 1. Cyclic voltammograms for an HOPG electrode immersed in the solutions employed for electrodeposition and electrooxidation (Figure 2) show a prominent oxidation peak that is associated with the oxidative removal of each material from the surface. These oxidation reactions are[32,33]

$$\text{Antimony: } Sb(s) + H_2O \rightarrow SbO^+(aq) + 2H^+ + 3e^- \quad (4)$$

$$Bi_2Te_3\text{: } Bi_2Te_3(s) + 6H_2O \rightarrow 3HTeO_2^+(aq) + 2Bi^{3+}(aq) + 9H^+ + 18e^- \quad (5)$$

$$\text{Gold: } Au(s) + 3Cl^- \rightarrow AuCl_3^{2-}(aq) + 1e^- \quad (6)$$

Note that, in all three cases, the products of the oxidation reactions are soluble. If oxidation is carried out using potentials well positive of this peak, a limiting rate for the oxidation reaction is imposed either by diffusion (e.g., Cl^- diffusion in the case of gold oxidation) or by the solubility of one or more products of the oxidation reaction.[34,35] On the negative edge of these oxidation peaks, in the limit of small anodic polarizations, the electrooxidation rate will be limited by the kinetics of the oxidation reaction, and the current density on the nanowire surfaces, J_{ox}, becomes constant.[31] The red arrows in Figure 2 indicate the potentials we employed for each material (Table 1). These optimum potentials were determined by trial and error, and in general, they represent the most positive potentials that satisfied the requirement that oxidation be kinetically controlled.

Multiple samples of nanowires were prepared using identical nucleation and growth parameters: E_{nucl}, t_{nucl}, E_{growth}, and t_{growth}.

TABLE 1: Parameters Employed for Nanowire Electrodeposition and Electrooxidation

material	E_{nucl},[a] t_{nucl}	E_{growth}, t_{growth}	I_{growth}[c]	E_{ox}	J_{ox}[d]
Sb	−1.0 V, 40 ms	−0.40 V, 75 s	500−1000 μA cm^{-2}	−0.060 V	137 μA cm^{-2}
Au	−1.0 V, 125 ms	0.45 V, 30 s	300−800 μA cm^{-2}	0.810 V	33.4 μA cm^{-2}
Bi_2Te_3	−0.6 V, 5 ms	n.a.[b]	n.a.[b]	0.370 V	109 μA cm^{-2}

[a] All potentials are referenced to a saturated calomel reference electrode (SCE). See Scheme 1 for a definition of the quantities: E_{nucl}, t_{nucl}, E_{growth}, t_{growth}, and E_{ox}. [b] Bi_2Te_3 nanowires were prepared using potentiodynamic electrodeposition as previously described.[12] [c] The range of the pseudo steady-state electrodeposition currents. These current values are normalized by the geometric area of the HOPG electrode. [d] The oxidation current density normalized by the area of the nanowires, calculated using eq 3 from the slopes of the plots shown in Figure 4.

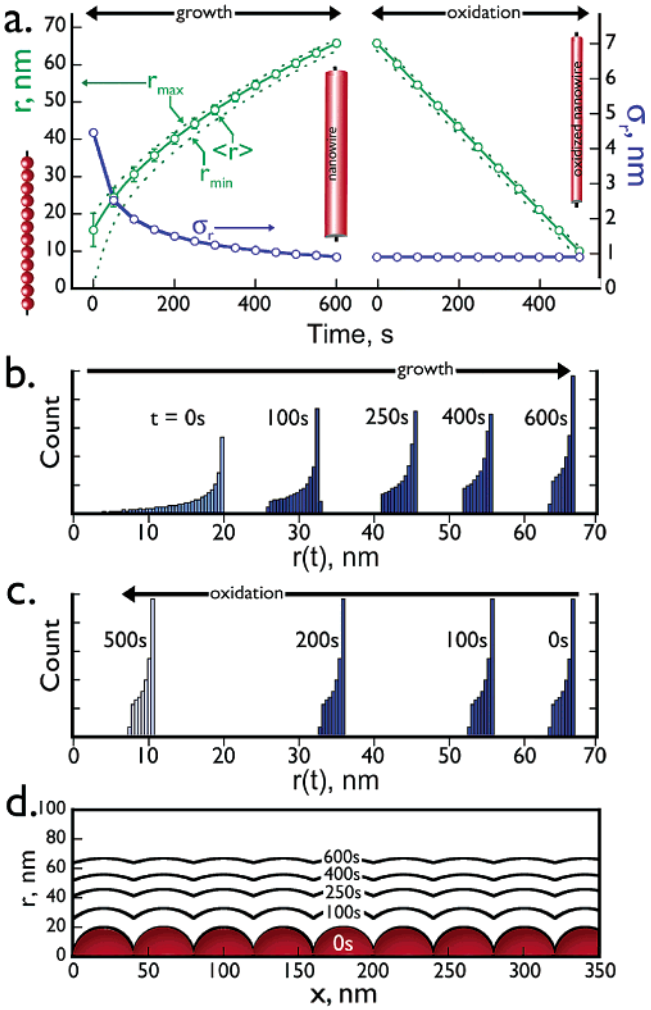

Figure 1. (a) Calculated mean nanowire radius, $\langle r \rangle$, and radius distribution vs time (green). Equations 1 and 3 were used to calculate $\langle r \rangle$ during growth and oxidation, respectively, starting with a nanowire consisting of hemispherical silver particles with a radius of 20 nm. Other parameters used in this calculation were the following: $i_{growth} = 1 \times 10^{-9}$ A cm^{-2}, $V_m = 10.26$ cm^3 mol^{-1}, $l = 1$ cm, $J_{ox} = 1 \times 10^{-4}$ A cm^{-2}. Dotted green lines show increase in radius for largest (r_{max}) and smallest (r_{min}) wire segments. The standard deviation of the radius, σ_r, vs time is plotted in blue. (b, c) Histogram of wire radii shown at several times during the deposition (b) and oxidation (c). (d) Radius vs axial distance profile of the nanowire as a function of growth time. The profile seen at 600 s is maintained throughout the oxidation process.

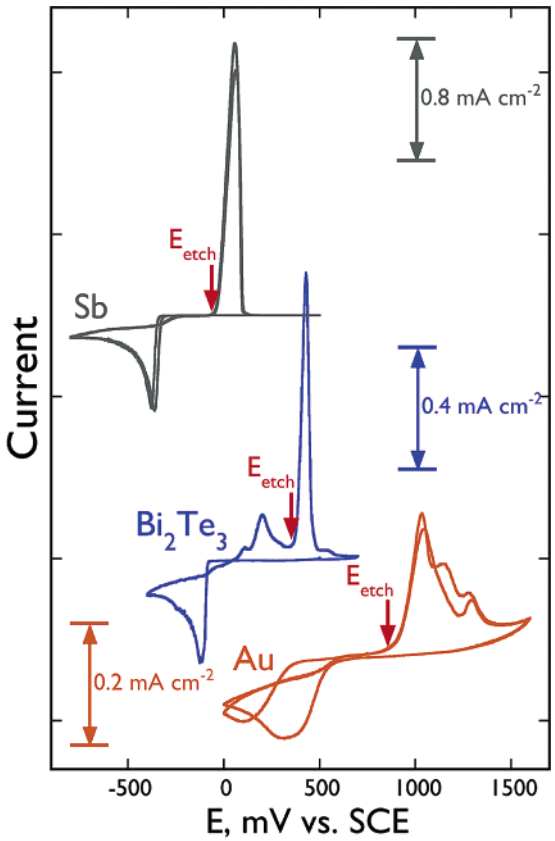

Figure 2. Cyclic voltammograms at 20 mV s^{-1} for an HOPG electrode immersed in the three solutions employed for electrodeposition and electrooxidation. For antimony, this solution was aqueous 5 mM $SbCl_3$, 0.1 M tartaric acid, and 0.1 M HNO_3. For gold: aqueous 2mM $AuCl_3$, 0.1 KCl, and 2 mM saccharin. For Bi_2Te_3: aqueous 1.5 mM $Bi(NO_3)_3$, 1.0 mM TeO_2, and 1 M HNO_3. The potentials employed for electrooxidation were −0.060 V vs SCE (Sb), 0.370 V (Bi_2Te_3), and 0.810 V (Au).

These nanowires were oxidized for various times, t_{ox}, using the same E_{ox}, listed in Table 1. The resulting nanowires were imaged using scanning electron microscopy, and representative images are shown in Figure 3. At left (Figure 3a,d,g) are shown nanowires of each composition before etching. The mean diameters of these wires were 120 ± 7 nm (Sb), 140 ± 10 nm (Bi_2Te_3), and 147 ± 11 nm (Au). The two images at right show wires subjected to an intermediate oxidation time (Figure 3b,e,h) and wires subjected to the longest oxidation times that preserved a 100 μm continuous wire length (Figure 3c,f,i). These SEM images show that a significant reduction of the wire diameter is achieved without a significant increase in the diameter heterogeneity, as compared with the initial state of the wire. It must be noted here that the oxidation current decreases with time and in direct proportion to the area of a nanowire and therefore in proportion to its radius (data not shown). We are unable to derive quantitative information from the oxidation current, because it contains contributions from the oxidation of both nanowires and nanoparticles. These nanoparticles, which can be seen in the SEMs of Figure 3, are produced in parallel with the growth of nanowires during the ESED synthesis process.

A statistical analysis of SEM data for more than 50 individual nanowires at each t_{ox} was compiled to prepare the plots shown in Figure 4. A plot of mean wire diameter versus t_{ox} (Figure 4a) shows that the decrease in wire diameter is directly proportional to t_{ox} for nanowires composed of all three materials,

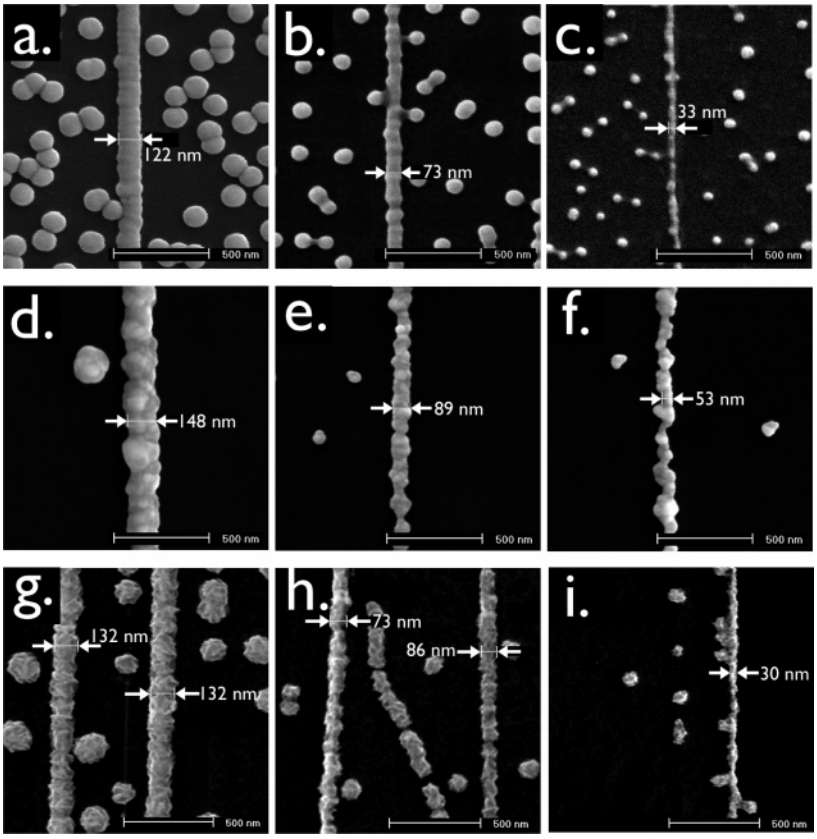

Figure 3. Representative scanning electron micrographs of antimony (a−c), gold (d−f), and Bi_2Te_3 (g−i) nanowires. (a) An antimony nanowire as-prepared using $E_{growth} = -0.40$ and $t_{growth} = 75$ s; and after electrooxidation at $E_{ox} = -0.060$ V for (b) 250 s and (c) 500 s. (d) A gold nanowire as-prepared using $E_{growth} = 0.45$ and $t_{growth} = 30$ s; and after electrooxidation at $E_{ox} = 0.810$ V for (e) 800 s and (f) 1300 s. (g) Bi_2Te_3 wires as-prepared using cyclic electrodeposition/stripping as previously described;[12] and after electrooxidation at $E_{ox} = 0.370$ V for (h) 400 s and (i) 800 s.

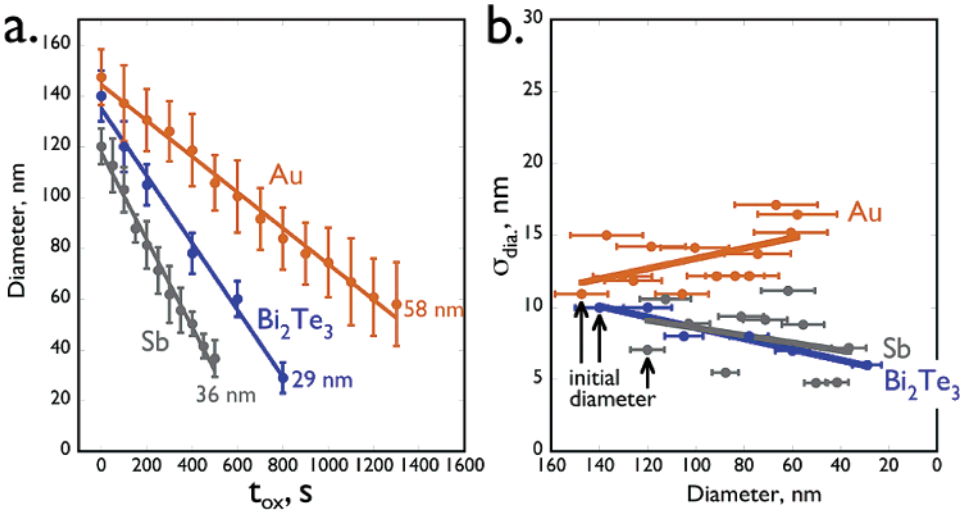

Figure 4. (a) Plots of mean nanowire diameter, ⟨dia.⟩, vs t_{ox} for gold, antimony, and Bi_2Te_3. Each data point plotted in (a) represents a separate nanowire growth experiment involving, for a particular material, nucleation and growth under the conditions specified in Table 1, followed by electrooxidation for various durations, t_{ox}. Distribution bars represent $\pm 1\ \sigma_{dia}$ for at least 50 diameter measurements for different wires on each surface. (b) Plot of the σ_{dia} vs ⟨dia.⟩ for each material.

as predicted by eq 3. The vertical error bars attached to the data points in Figure 4a are $\pm 1\sigma_{dia}$. We also plot σ_{dia} versus t_{ox} separately in Figure 4b. The changes in σ_{dia} seen here (a slight reduction for Sb and Bi_2Te_3 and a slight increase for Au) are too small to be statistically significant. Both the linearity of the diameter versus t_{ox} data and the independence of σ_{dia} on t_{ox} are consistent with a kinetically controlled electrooxidation process modeled by eq 3. The data shown in Figure 4 further demonstrate that electrochemical wire growth (by ESED) and shrinking by electrooxidation can be integrated into a single electrochemical experiment that permits the final mean diameter of nanowires to be specified with a precision of 5−10 nm. The nanowire length, as well as its diameter, is reduced by electrooxidation, and this reduction in length is approximately equal to the absolute change in the wire radius. Since the largest radius change achieved here is ≈50 nm, and since the nanowires

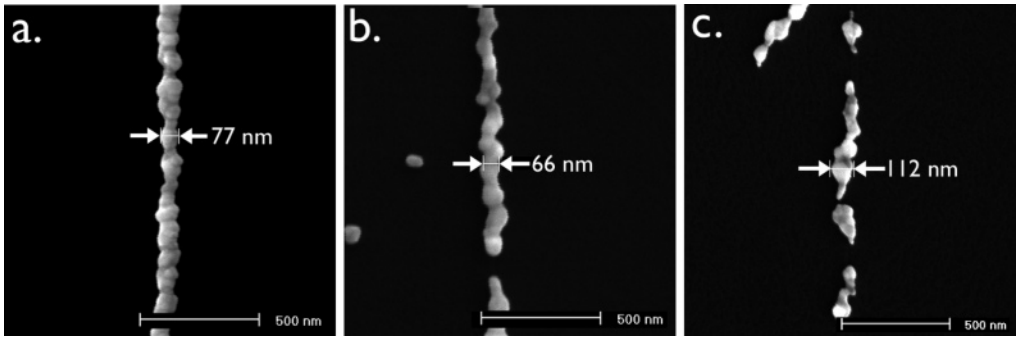

Figure 5. Scanning electron micrographs of gold nanowires after the removal, by electrooxidation, of nearly identical quantities of gold (Q_{ox} = 965−1000 μC cm^{-2}) using three different electrooxidation potentials. The initial diameter of all three wires was 147 ± 11 nm. (a) E_{ox} = 0.810 V vs SCE, t_{ox} = 1000 s, Q_{ox} = 968.9 μC cm^{-2}. These wires remained continuous for more than 100 μm. (b) E_{ox} = 0.825, t_{ox} = 600 s, Q_{ox} = 967.4 μC cm^{-2}. These wires had continuous sections 1−5 μm in length. (c) E_{ox} = 0.837 V, t_{ox} = 300 s, Q_{ox} = 1000.2 μC cm^{-2}. The longest continuous wire sections were ∼500 nm in length.

employed here are more than 100 μm in length, this reduction in length of <0.1% is insignificant. It should also be noted that the Bi_2Te_3 nanowires investigated here are microcrystalline,[12] and it is reasonable to expect variations in the kinetically controlled oxidation rate with the crystallographic orientation of the facets for individual microcrystals. In principle, this effect could cause nanowires to etch anisotropically and to undergo roughening. However, the SEM data shows that this effect is insignificant for Bi_2Te_3 nanowires. It is unlikely that this isotropic etching behavior would be observed for microcrystalline nanowires more generally, and this represents a clear limitation of this methodology.

Wire uniformity was retained during electrooxidation only for E_{ox} values more negative than those compiled in Table 1 (i.e., slower oxidation rates). Higher oxidation rates, obtained using more positive values for E_{ox}, caused pronounced surface roughening and the generation of breaks in the nanowires during electrooxidation. Gold nanowires oxidized at three different E_{ox} values (0.810 V (a), 0.825 V (b), and 0.837 V (c)) are shown in the SEM images of Figure 5. In this experiment, the mean diameter of the gold nanowires before oxidation was 147 ± 11 nm, and the oxidation charge, Q_{ox}, was nearly constant and equal to 950−1000 μC cm^{-2}. Even though these three potentials span just 27 mV, dramatically different behavior was seen at 0.837 V where oxidation required just 300 s (versus 1000 s at 0.810 V), and the longest continuous wire sections after oxidation were ≈500 nm (versus 100 μm at 0.810 V). Gold wires oxidized at 0.825 required 600 s for oxidation and showed continuous sections 1−5 μm in length.

IV. Summary

Kinetically controlled electrooxidation provides a means for reducing the diameter of nanowires without degrading the wire diameter uniformity. This method can be applied to nanowires prepared using any method and having any composition, provided that oxidation can be effected electrochemically and that the products of the oxidation are soluble. Kinetically controlled electrooxidation can be coupled with the ESED method of nanowire synthesis to allow the preparation of nanowires with diameters in the range from 20 to 50 nm.

Acknowledgment. This work was funded by the National Science Foundation (grant CHE-0111557) and the Petroleum Research Fund of the American Chemical Society (grant 40714-AC5). We also acknowledge financial support for M.A.T. from the Integrated Micro/Nano Summer Undergraduate Research Experience (or IM-SURE) program administered by the Undergraduate Research Opportunities Program (UROP) at UCI. Graphite for this work was supplied by a grant from the EU Commission FP6 NMP-3 project 505457-1, titled "ULTRA-1D".

References and Notes

(1) Cui, Y.; Wei, Q. Q.; Park, H. K.; Lieber, C. M. *Science* **2001**, *293*, 1289.

(2) Favier, F.; Walter, E. C.; Zach, M. P.; Benter, T.; Penner, R. M. *Science* **2001**, *293*, 2227.

(3) Hahm, J.; Lieber, C. M. *Nano Lett.* **2004**, *4*, 51.

(4) Kolmakov, A.; Zhang, Y. X.; Moskovits, M. *Nano Lett.* **2003**, *3*, 1125.

(5) Liu, H. Q.; Kameoka, J.; Czaplewski, D. A.; Craighead, H. G. *Nano Lett.* **2004**, *4*, 671.

(6) Murray, B. J.; Newberg, J. T.; Walter, E. C.; Li, Q.; Hemminger, J. C.; Penner, R. M. *Anal. Chem.* **2005**, *77*, 5205.

(7) Johnson, J. C.; Yan, H. Q.; Yang, P. D.; Saykally, R. J. *J. Phys. Chem. B* **2003**, *107*, 8816.

(8) Yan, H. Q.; He, R. R.; Johnson, J.; Law, M.; Saykally, R. J.; Yang, P. D. *J. Am. Chem. Soc.* **2003**, *125*, 4728.

(9) Johnson, J. C.; Yan, H. Q.; Schaller, R. D.; Haber, L. H.; Saykally, R. J.; Yang, P. D. *J. Phys. Chem. B* **2001**, *105*, 11387.

(10) Huang, M. H.; Mao, S.; Feick, H.; Yan, H. Q.; Wu, Y. Y.; Kind, H.; Weber, E.; Russo, R.; Yang, P. D. *Science* **2001**, *292*, 1897.

(11) Heremans, J.; Thrush, C. M.; Lin, Y. M.; Cronin, S.; Zhang, Z.; Dresselhaus, M. S.; Mansfield, J. F. *Phys. Rev. B* **2000**, *61*, 2921.

(12) Menke, E. J.; Li, Q.; Penner, R. M. *Nano Lett.* **2004**, *4*, 2009.

(13) Prieto, A. L.; Martin-Gonzalez, M.; Keyani, J.; Gronsky, R.; Sands, T.; Stacy, A. M. *J. Am. Chem. Soc.* **2003**, *125*, 2388.

(14) Prieto, A. L.; Sander, M. S.; Martin-Gonzalez, M. S.; Gronsky, R.; Sands, T.; Stacy, A. M. *J. Am. Chem. Soc.* **2001**, *123*, 7160.

(15) Sander, M. S.; Gronsky, R.; Sands, T.; Stacy, A. M. *Chem. Mater.* **2003**, *15*, 335.

(16) Fan, Z. Y.; Chang, P. C.; Lu, J. G.; Walter, E. C.; Penner, R. M.; Lin, C. H.; Lee, H. P. *Appl. Phys. Lett.* **2004**, *85*, 6128.

(17) Kind, H.; Yan, H. Q.; Messer, B.; Law, M.; Yang, P. D. *Adv. Mater.* **2002**, *14*, 158.

(18) Li, Q. G.; Penner, R. M. *Nano Lett.* **2005**, *5*, 1720.

(19) Wang, J. F.; Gudiksen, M. S.; Duan, X. F.; Cui, Y.; Lieber, C. M. *Science* **2001**, *293*, 1455.

(20) Zhang, D.; Li, C.; Han, S.; Liu, X.; Tang, T.; Jin, W.; Zhou, C. *Appl. Phys. A* **2003**, *77*, 163.

(21) Melosh, N. A.; Boukai, A.; Diana, F.; Gerardot, B.; Badolato, A.; Petroff, P. M.; Heath, J. R. *Science* **2003**, *300*, 112.

(22) Morales, A. M.; Lieber, C. M. *Science* **1998**, *279*, 208.

(23) Pan, Z. W.; Dai, Z. R.; Wang, Z. L. *Science* **2001**, *291*, 1947.

(24) Trentler, T. J.; Hickman, K. M.; Goel, S. C.; Viano, A. M.; Gibbons, P. C.; Buhro, W. E. *Science* **1995**, *270*, 1791.

(25) Zach, M. P.; Ng, K. H.; Penner, R. M. *Science* **2000**, *290*, 2120.

(26) Savolainen, M.; Touboltsev, V.; Koppinen, P.; Riikonen, K. P.; Arutyunov, K. *Appl. Phys. A* **2004**, *79*, 1769.

(27) Walter, E. C.; Zach, M. P.; Favier, F.; Murray, B. J.; Inazu, K.; Hemminger, J. C.; Penner, R. M. *ChemPhysChem* **2003**, *4*, 131.
(28) Walter, E. C.; Murray, B. J.; Favier, F.; Kaltenpoth, G.; Grunze, M.; Penner, R. M. *J. Phys. Chem. B* **2002**, *106*, 11407.
(29) i_{growth} is the total measured current during electrodeposition normalized by the geometrical area of the electrode.
(30) J_{ox} is the electrooxidation current normalized by the area of the hemicylindrical nanowires present within 1 cm^2 of geometrical electrode area.
(31) Bard, A. J.; Faulkner, L. R. *Electrochemical Methods: Fundamentals and Applications*, 2nd ed.; John Wiley & Sons: New York, 2001.
(32) Martin-Gonzalez, M. S.; Prieto, A. L.; Gronsky, R.; Sands, T.; Stacy, A. M. *J. Electrochem. Soc.* **2002**, *149*, C546.
(33) Pourbaix, M. *Atlas of Electrochemical Equilibria in Aqueous Solutions*; Cebelcor: Brussels, 1974.
(34) Davydov, A. D. *Sov. Electrochem.* **1991**, *27*, 835.
(35) Davydov, A. D. *Electrochim. Acta* **1998**, *43*, 29.